AIAA JOURNAL
Vol. 38, No. 7, July 2000

Modeling Hail Ice Impacts and Predicting Impact Damage Initiation in Composite Structures

Hyonny Kim* and Keith T. Kedward†
University of California, Santa Barbara, Santa Barbara, California 93106

Hail ice impacts are a realistic threat to exposed composite structures such as aircraft fuselage and wing skins, leading-edge and control surfaces, engine nacelles, and fan blades. To shed some light onto this little-understood (and unavoidable) threat, experimental, numerical, and analytical investigations have been conducted. Experiments in which carbon/epoxy composite panels were impacted by ice spheres at high velocity (30–200 m/s) were conducted to measure 1) the impact energy at which damage initiates, 2) the multiple failure modes exhibited by thin composite panels over a range of impact velocity, and 3) the elastic response of a composite panel resulting from impact. Subsequent numerical analyses of the last case were performed and were validated through correlation with experimental data. Insights gained from the numerical analyses were used to compose a mechanics-based formula that predicts the initiation of damage formation. This formula, derived using a global energy balance, provides a cost-effective (i.e., lower number of tests needed) means by which the impact damage resistance of composite structures and material types can be established.

Introduction

LAMINATED polymer composites have found widespread use in the design of aerospace structures. Although these materials offer excellent in-plane performance, they are susceptible to damage when severely loaded out-of-plane, such as in the case of localized impacts. Often the damage resulting from impacts is barely visible and exists in the form of subsurface matrix cracks, backside fiber failure, and delaminations. The latter two damage forms can significantly degrade a structure's performance. This paper focuses on the transverse impact of flexible composite structures by high-velocity (30–200 m/s) hail ice, a realistic threat that exists both while in-flight and on the ground. Much of the previous work has focused on the impact of thick composite plates by low-velocity metallic impactors[1–7] that behave elastically during the impact event. As a high-velocity projectile, however, ice exhibits significant permanent deformation and microcracking induced by crushing[8] and is a material for which mechanical properties are still currently under investigation.[9,10]

Because the existence of barely visible impact damage can be a significant safety threat, the capability to predict such damage is of great utility. The objective of this paper, therefore, is to demonstrate a method that predicts the initial formation of damage in thin-walled composite structures due to high-velocity hail ice impacts. This method is formulated analytically, using a global energy balance and is founded on assumptions drawn from insights provided by detailed numerical simulations of ice impacting composite panels. These simulations are validated through correlation with experimental data and observations.

Presented within this paper is the description of experimental investigations (previously conducted by Kim[11]), numerical simulations, and the formulation of a method for predicting impact damage initiation. In the simulations, a model representing the material behavior of ice as an impact projectile is first needed to confidently predict ice impacts on structures. Therefore, the modeling of ice impacts onto an instrumented metal target has also been undertaken and is reported herein.

Received 26 June 1999; revision received 13 November 1999; accepted for publication 29 November 1999.

*Postdoctoral Fellow, Department of Mechanical and Environmental Engineering. Member AIAA.
†Professor, Department of Mechanical and Environmental Engineering. Fellow AIAA.

Experiments

To investigate the hail ice impact threat, a nitrogen gas cannon, shown schematically in Fig. 1, was used to project simulated hail ice (SHI) spheres of construction shown in Fig. 2. The monolithic ice spheres were cast in a split spherical mold over 1 filling session, and the flatwise layered spheres were constructed by casting over 10–11 filling sessions. The motivation for using a layered ice sphere was to produce a projectile that was more representative of hail ice. Actual hail ice has a spherically layered construction composed of many thin layers and is significantly tougher than monolithic ice. The sizes of SHI tested were 25.4, 42.7, and 50.8 mm in diameter.

The experimental investigation can be categorized by the two target types tested: 1) a force measurement transducer (FMT) system and 2) composite panels.

Ice Impact Force Measurements

The FMT, shown in Fig. 3, consists of a commercially available dynamic force transducer (piezoelectric ring) mounted between a titanium platen and a thick steel plate. The FMT measures the dynamic force history of an ice sphere during its impact contact with a rigid target to assist in understanding the impact behavior of ice and the effect of parameters such as construction, size, and velocity. High-speed film photography (11,000 frames per second) was used to observe the kinematic behavior of the ice during the impact event.

A typical impact force history, measured by the FMT, is shown in Fig. 4a. This particular test is for a 42.7-mm layered SHI sphere impacting the FMT at 73.5 m/s. The total window of time shown is 1 ms, during which a peak contact force of 15.9 kN (3570 lbf) was recorded. Also in Fig. 4 are two still images from high-speed film taken of this same test (note that the time associated with each photograph is indicated on the horizontal axis of Fig. 4a). As seen in the photographs, the ice sphere locally crushes immediately on contact with the FMT face and proceeds to fail locally during the impact event. Matching the time of the photograph in Fig. 4b (91 μs after impact) with the time of peak force (98 μs), it is evident that only a small portion of the sphere's volume has disintegrated by the time of peak force. Note also how the portion of the sphere that has been dyed blue (central band) whitens as the event proceeds. This is evidence of microcracking throughout the sphere. The same localized crushing behavior of ice spheres impacting a rigid target at high velocities was also reported by Singh et al.[8]

A total of 31 force measurement experiments involving normal impacts of SHI onto the FMT were conducted over a range of test parameters. The results of these tests are summarized in a following section, together with the results of the numerical simulations, in the

Table 1 FTE level for AS4/8552 and AS4/977 panels

Panel thickness, mm	Weave[a]/resin	Layup	Failure threshold energy, J, for ice diameter		
			25.4 mm	42.7 mm	50.8 mm
1.22	8HS/8552	$[0/45]_s$	56	115, 129, 119	111, 114
1.83	8HS/8552	$[0/45/90]_s$	N/A[b]	190, 195, 202	N/A[b]
2.44	8HS/8552	$[0/45/90/-45]_s$	95	250, 254	318
1.42	5HS/977	$[0/45/90]_s$	N/A[b]	122	N/A[b]
1.91	5HS/977	$[0/45/90/-45]_s$	84	199, 210	N/A[b]
2.62	5HS/977	$[0/45/90/-45/0/45]_s$	N/A[b]	277	380

[a]Fabric weave styles: 8 HS = eight-harness satin, 5 HS = five-harness satin.
[b]Data not available due to experimental condition not tested.

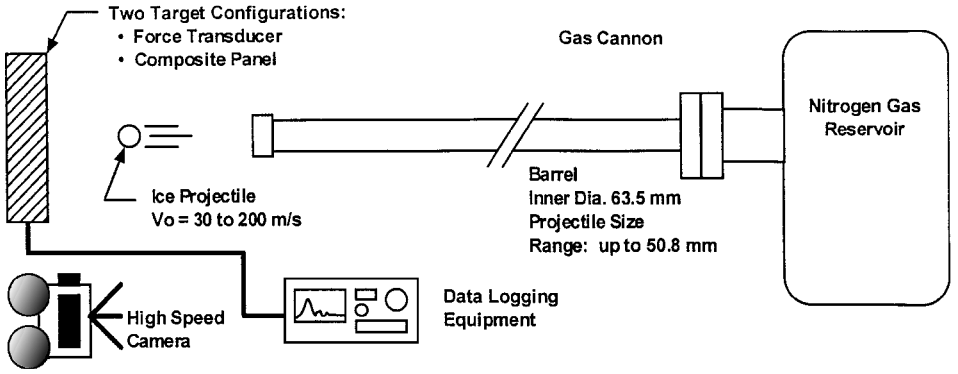

Fig. 1 Nitrogen gas cannon experimental setup.

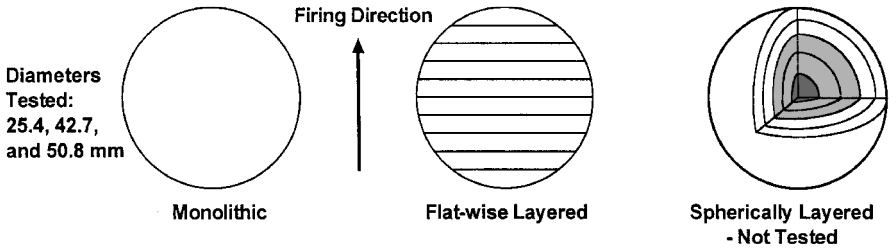

Fig. 2 SHI construction; monolithic or layered.

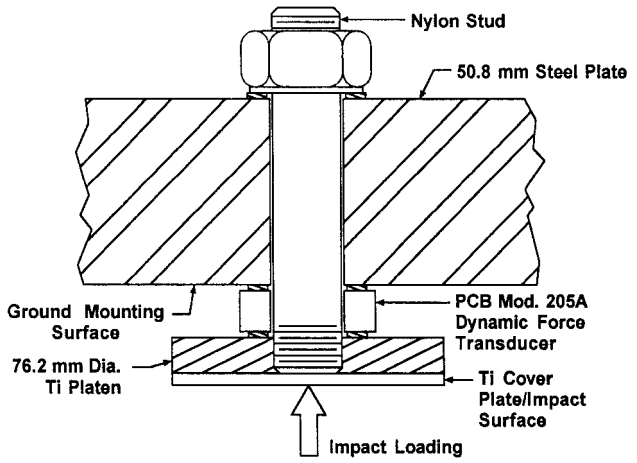

Fig. 3 FMT target.

form of an observed linear trend in peak force vs projectile kinetic energy.

Composite Panel Impacts

A series of experiments involving normal impacts onto composite panels were performed to measure 1) the impact energy at which damage initiates, 2) the failure modes exhibited by composite panels impacted by ice, and 3) the elastic response of thin-gauge composite panels when impacted by ice. As shown in Fig. 5, the composite panel targets were held firmly by an aluminum fixture. Note the details of the panel boundary conditions. The aluminum picture frame fixture employs silicone rubber gaskets at the panel boundary to provide a uniform clamping pressure that was not so high that it restricted in-plane movement of the panel when it responded to the impact. The compliance of this gasket, however, resulted in a boundary that was not perfectly clamped, particularly with respect to the slight rotation permitted at the panel boundary.

All panels were AS4/8552 and AS4/977 carbon/epoxy fabric plates, in eight- and five-harness-satin weave styles, respectively. The layup and thickness of the panels is given in Table 1. The experimentally measured failure threshold energy (FTE) for each panel and ice diameter combination is also summarized in Table 1. FTE is defined as the lowest kinetic energy of the incoming projectile coinciding with the incidence of damage to a laminated composite panel. Below this kinetic energy level, impacts onto a panel target produce no apparent damage. The delamination failure mode was observed for impacts at energy levels slightly above the FTE. This was also identified as the initial failure mode in the work by Elber.[12] The FTE is dependent on both panel thickness and ice diameter. For several thickness/diameter combinations, duplicate tests were performed, producing multiple data points for the same test condition by which to ascertain the repeatability of the measured FTE data. Note that the carbon/epoxy fabric panels tested all had quasi-isotropic-type layups, effectively resulting in bending stiffness (as calculated by laminated plate theory) that is dependent only on thickness, much like isotropic plates.

Impact experiments were conducted to determine the multiple damage modes exhibited by the composite panels under ice impact

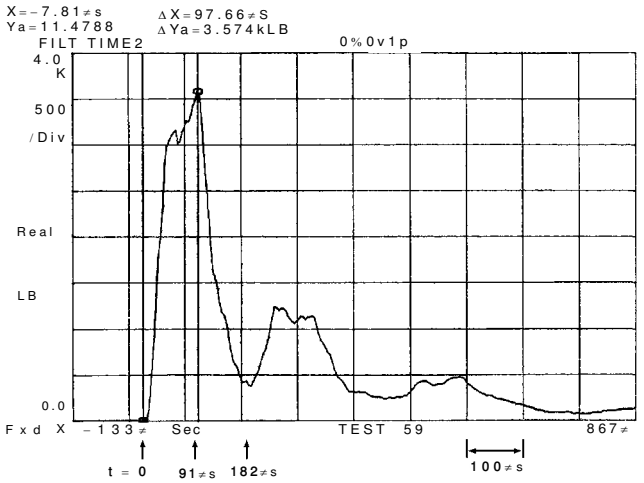

a) Force time history trace from digital storage oscilloscope, peak force 15.9 kN (3570 lbf)

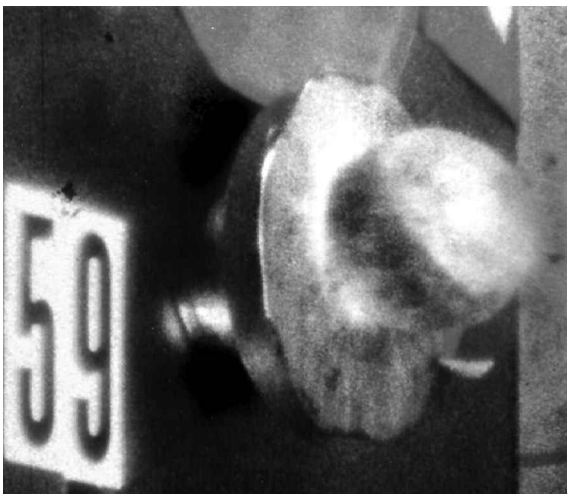

b) Still image at 91 θs after impact

c) Still image at 182 θs after impact

Fig. 4 Experimental record of test 59; 42.7-mm-diam layered SHI impacting FMT at 73.5 m/s.

loading. Shown in Fig. 6, a progression of failure modes was observed over a range of impact threat levels. Figure 6 highlights an important experimental observation: The severity of damage does not always increase with threat, especially with regard to a structure's damage tolerance. A more threatening impact (i.e., higher velocity for given mass) could result in a damage mode, type II, for example, that is potentially less detrimental to structural performance than a failure mode caused by an impact of lower threat (i.e., lower velocity), type I, for example. To illustrate this point, compare the post-impact integrity of a structure having damage produced by a higher threat impact (types II or III) for which backside fiber failure or through-thickness cracks result, with a lower threat impact (type I) for which extensive delaminations occur. The through-thickness cracks can be less susceptible to propagation under tension loading than the corresponding delamination under compression loading.

A thorough study of failure mode progression over a range of impact velocities is important because structural validation tests are often performed using only a single velocity based on the maximum perceived threat. This approach potentially overlooks some failure modes that are excited by lower velocity impacts, the danger being that such failure modes can be more severe than those produced by tests of higher velocity, as illustrated in Fig. 6. Note that glancing impacts have been found to act as normal impacts with an effective energy equal to a quantity calculated from the total kinetic energy scaled by the target surface normal vector component.[11,13] Note that from ice force measurement tests it has been determined that energy is directly proportional to force and, thus, total kinetic energy can be treated as a vectorlike quantity. This reinforces the need to perform impact tests over a range of velocities to capture all failure modes, particularly because most in-flight impacts would be of a glancing nature.

A series of experiments involving impacts of strain gauge instrumented composite panels were also conducted to carefully measure the panel's undamaged elastic response. These experiments are discussed in detail in the following section, together with the results of the numerical simulations.

Finite Element Simulations

Ice Material Model Validation

The impact of high-velocity spherical ice projectiles onto composite panels was simulated using the explicit finite element (FE) code DYNA3D (Ref. 14). In preparation for this numerical simulation, significant effort was first put into developing a suitable model for the ice projectile itself. To accomplish this, the FMT geometry was carefully modeled, using the quarter-symmetric mesh shown in Fig. 7. The intent of the model was to predict the experimentally measured force time history, and thus demonstrate that a suitable ice model has been developed. The model includes all components of the system except for the thick steel plate and the nut at the end of the nylon stud (see Fig. 3). At the piezoelectric ring to steel plate interface, nonreflecting and appropriately fixed boundary conditions were specified. The nonreflecting boundary condition did not permit the reflection of stress waves when they reached this boundary.

Of primary interest are the material properties used in modeling the ice sphere. An existing material model was employed, that being the DYNA3D material type 13 elastic–plastic with failure. This model allowed for hardening plastic behavior that is shown (by results to be presented) to adequately account for the ice microcrack evolution[10] just prior to achieving a crushed powder, fluidlike state. Table 2 summarizes the basic material inputs used in this model. Properties such as shear modulus and bulk modulus were taken from the literature.[15–17] Values for hardening modulus, plastic failure strain, and failure pressure (negative value denotes tensile hydrostatic stress) were parametrically determined by comparing the numerical simulation results with the experimental data. Finally, the density was a direct measurement of the tested SHI weight divided by the spherical volume; a mean value of recorded density was used in the numerical simulations. The behavior of this

Table 2 Ice material input for DYNA3D material type 13 elastic–plastic with failure model

Property	Value
Density, kg/m^3	846
Elastic shear modulus, GPa	3.46
Yield strength, MPa	10.3
Hardening modulus, GPa	6.89
Bulk modulus, GPa	8.99
Plastic failure strain, %	0.35
Tensile failure pressure,[a] MPa	−4.00

[a]Negative value denotes hydrostatic tension stress.

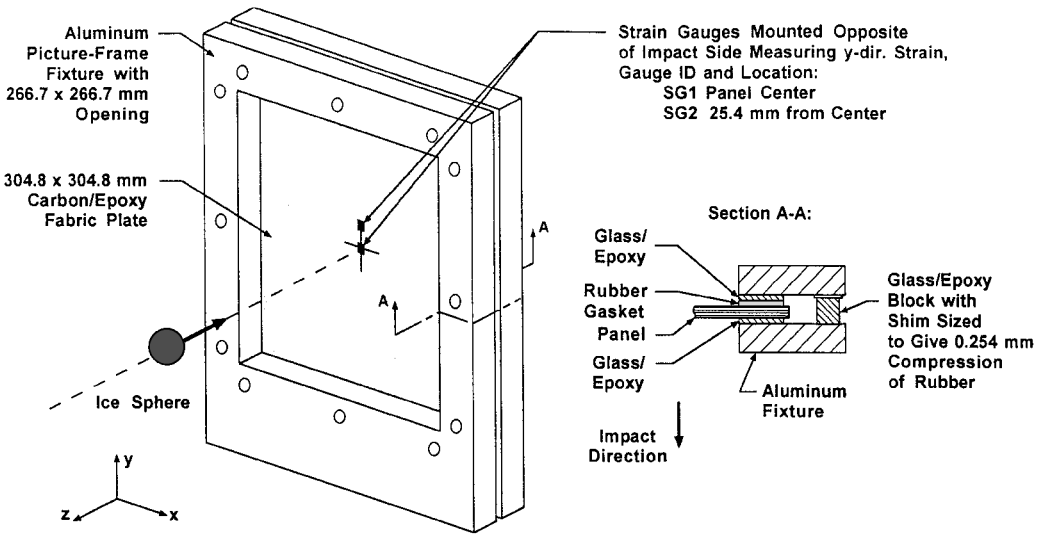

Fig. 5 Composite panel target and fixture cross-sectional detail.

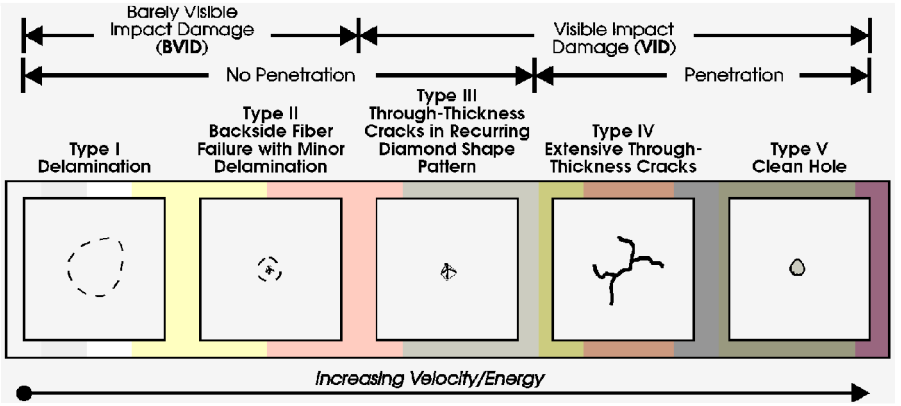

Fig. 6 Failure modes observed experimentally for high-velocity ice impacts.

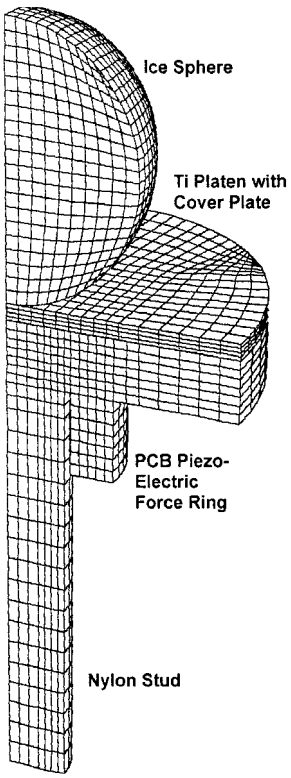

Fig. 7 Quarter-model mesh of 42.7-mm-diam ice sphere impacting FMT.

material model is such that when the plastic failure strain is reached, all shear stress components are relaxed to zero. Furthermore, when the tensile failure pressure is reached, the material is only allowed to carry hydrostatic compressive stress, thus behaving like a fluid. Note that this is a simplified material model representation of such a complex material as ice. Researchers show ice to be quite complicated, as it exhibits a nonlinear pressure–volume[17,18] relationship as well as failure strength dependency on strain rate[9,19] and confining pressure.[20] In the numerical analyses, the use of the DYNA3D type 13 elastic–plastic with failure material model results in material behavior that has a linear pressure–volume relationship and does not exhibit any dependency of ice failure strength on strain rate and pressure.

Figure 8 shows the deformed mesh of a DYNA3D model simulating the impact of 42.7-mm-diam SHI onto the FMT at 73.5 m/s. Comparing Figs. 8 and 4, one can observe that the simulation captures the kinematic behavior of the ice impact experiments. Failed material flowing outwards from the impact site is predicted by the DYNA3D simulation, with the shape of the projectile remaining largely spherical except for the volume local to the contact region.

Figure 9 shows the numerically predicted force history compared with data from four different tests of SHI impacting the FMT. As seen in Fig. 9, the peak forces and general force pulse shapes were predicted by DYNA3D moderately well in each case. The major discrepancy lies in the numerically predicted time to peak force occurring before the experimentally measured time to peak. This error in prediction is partially due to the chosen location at which contact force information was gathered from the DYNA3D simulations. Contact force was gathered at the ice sphere-to-platen interface,

whereas the experimental data were the volume averaged strain measurement taken by the piezoelectric force ring. Thus, the numerically predicted force history shows an immediate rise after first contact, unlike the experimental data that have a more gradual initial rise due to the finite time needed for stress waves to pass through the platen and compress the force ring.

A total of five different velocity impact simulations were run with DYNA3D. These are summarized in Fig. 10 in the form of numerically predicted peak force vs projectile kinetic energy. Also in Fig. 10 are plotted data for all tests involving SHI (both monolithic and layered, all three diameters) impacting the FMT. The relationship between measured peak force and projectile kinetic energy was found to be linear regardless of ice size for impacts of a high-velocity nature, that is, having similar localized ice failure attributes. In Fig. 10, it is clear that the DYNA3D predictions follow the trend experimentally measured for monolithic SHI. This is an expected result as the DYNA3D model does not account for layered ice construction and is, therefore, a model of the monolithic SHI. Note, however, that the behavior of the two types of SHI lie within

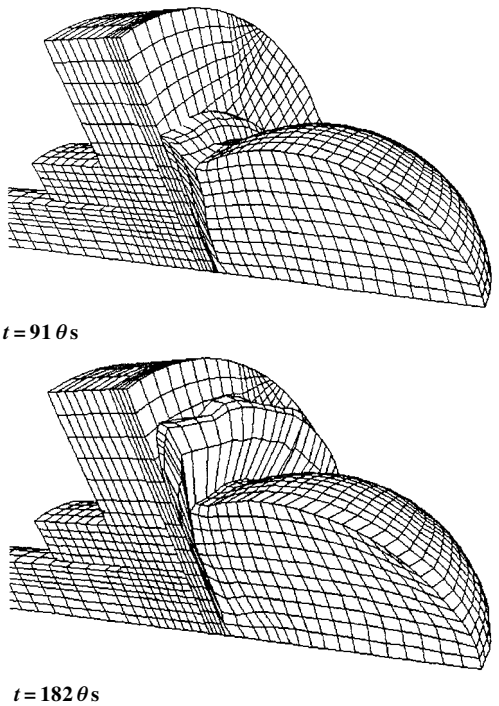

Fig. 8 Simulation of test 59; 42.7-mm-diam layered SHI at 73.5 m/s.

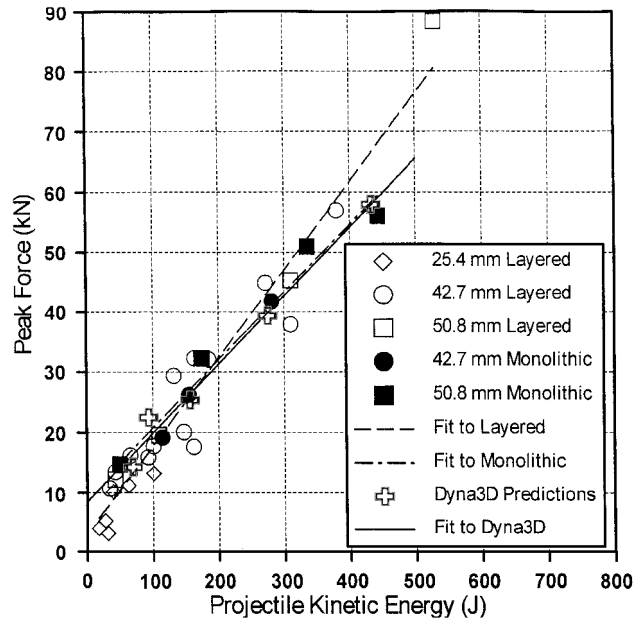

Fig. 10 Summary of peak forces for all SHI on FMT tests along with DYNA3D results.

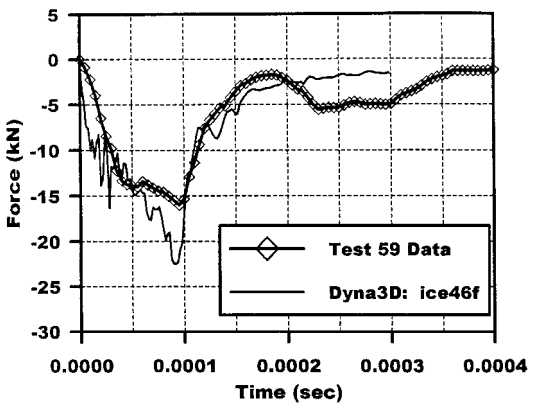

Test 59: 42.7-mm layered SHI at 73.5 m/s

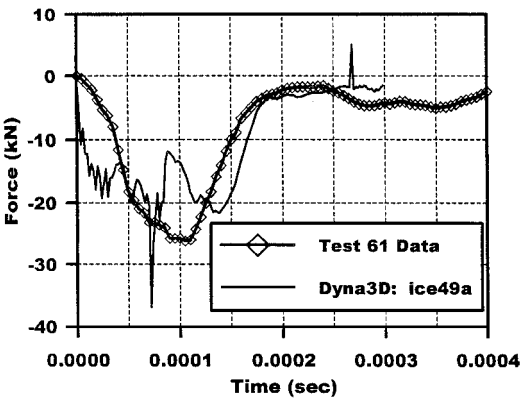

Test 61: 42.7-mm monolithic SHI at 95.4 m/s

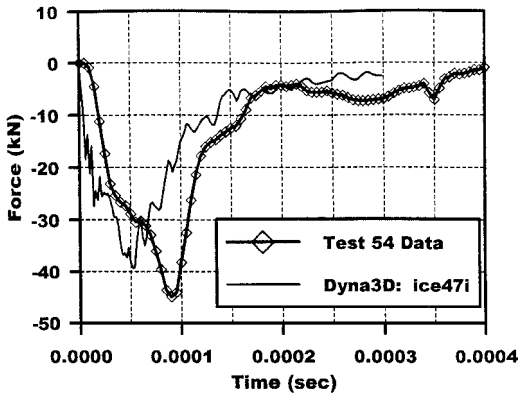

Test 54: 42.7-mm layered SHI at 126 m/s

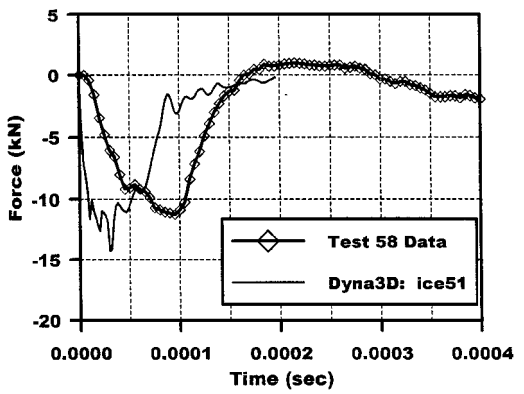

Test 58: 25.4-mm layered SHI at 139 m/s

Fig. 9 Force history predictions of SHI impacting FMT: multiple cases.

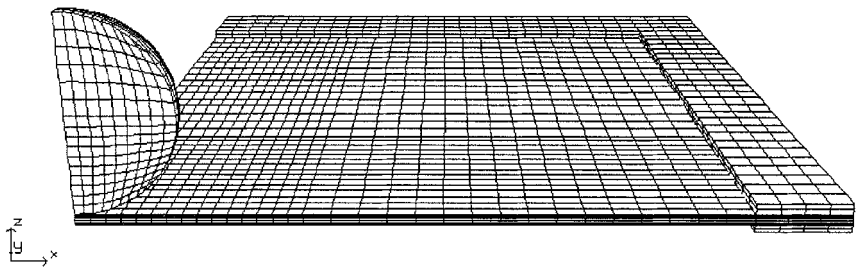

Fig. 11 Mesh of 42.7-mm-diam SHI impacting composite panel.

Table 3 Experimental test cases simulated by DYNA3D

Test Number	Panel thickness, mm	Ice diameter, mm	Velocity, m/s	Kinetic energy, J	Test result	Peak strain SG1, $\mu\varepsilon$	Time to peak, μs	DYNA3D model Identification
137	2.44	42.7	73.2	95	No damage	10,350	77	pan15b
138	2.44	25.4	154	84	No damage	11,870	74	pan18c

the experimental scatter of each other up to an impact energy of 400 J. Thus, the numerical model is an adequate representation for both SHI types within this range.

A final point of discussion is needed regarding the SHI impacts on FMT tests and simulation results. The measured forces for the case of ice impacting a rigid titanium platen target can in no way be directly used to state what the load magnitude would be for the case of ice impacting a real structure (significantly more compliant than the platen). The tests involving the FMT as a target are primarily a calibration used for quantitatively describing the ice's behavior and also serve as a benchmark for analytical correlation (validation). With little exception, when ice (or any low-mass, small projectile) impacts a real structure, the contact force cannot be directly measured experimentally without significantly disturbing the target or altering the projectile. Validated simulation currently remains as the only means by which contact force information can be predicted. Such contact force information is useful in the design of structures and as a parameter for predicting a structure's damage resistance.[1]

Ice Model Application: Panel Impact Simulation

A reliable model for ice has been developed and is now applied to predicting the dynamic response of a composite panel impacted by high-velocity SHI. The motivation for such an undertaking is to support the development of an analytical model (i.e., closed form) that predicts impact damage formation. Although numerical simulations predicting panel failure and even the extent of failure have not been accomplished to date by the authors, DYNA3D simulations of ice impacting composite panels can be used to determine the stress state that is built up just prior to damage initiation. The DYNA3D simulations presented here, therefore, involve a highly deformable ice projectile impacting a panel target that deforms only within the elastic range.

The DYNA3D mesh shown in Fig. 11 is of a 42.7-mm ice sphere impacting a 2.44-mm-thick, 8-ply panel. This quarter-symmetric model, having 10,284 8-node solid elements, employs 7 layers of elements, one for each ply (or grouping), to model the panel. Each layer was given the following orthotropic elastic properties, with the ply angle specified on a layer-to-layer basis: $E_{11} = 71.7$, $E_{22} = 69.5$, and $E_{33} = 6.89$ GPa; $G_{12} = 5.17$, $G_{23} = 5.17$, and $G_{13} = 5.17$ GPa; and $\nu_{21} = 0.038$, $\nu_{31} = 0.029$, and $\nu_{32} = 0.030$. Solid elements were used instead of shell elements due to the shell element's inability to exactly calculate through-the-thickness stress components. These through-the-thickness, or interlaminar in the case of laminated composites, stress components are essential for the prediction of the delamination failure mode. The model incorporates the impact ice material model discussed earlier. The ice sphere was given only a velocity initial condition, thus relying on the defined contact surfaces to account for the sphere-to-panel interaction. Note in Fig. 11 that the details of the panel boundary (i.e., the silicone rubber gasket and glass/epoxy blocks with frictional sliding interfaces) needed to be modeled to correctly predict the long-term panel center deflection history response.

Two experimental test cases simulated using DYNA3D are summarized in Table 3. Listed for each case are the test identification number, panel thickness, ice diameter, kinetic energy, measured peak strain, and the time to reach peak strain. The strain gauges are located at the panel center (labeled SG1), exactly opposite of the impact location, and 25.4 mm from the center (labeled SG2) as shown in Fig. 5. The DYNA3D models used for simulating these tests are also listed in Table 3. In the tests, the SHI velocity was purposely selected such that no damage was incurred by the composite panel, and, therefore, the same panel was used for both tests. This 2.44-mm-thick panel has an 8-ply quasi-isotropic layup, $[0/45/90/-45]_s$. In addition to the strain gauge instrumentation, high-speed film photography was taken of the impact event from which the panel center deflection time history was measured.

Figure 12 shows the predicted panel center deflection along with the experimentally measured center deflection history for test 137. Also shown in Fig. 12 are the predicted contact force history at the sphere-to-panel interface and an enlarged time-scale plot showing the times at which predicted bending strain (SG1) and interlaminar shear (ILS) stress are maximum. The time axes of the force and displacement plots are aligned to assist in understanding the kinematics of the event. The SHI loads up the panel center, which quickly deforms and eventually accelerates away from the impacting ice mass, as exhibited by the momentary loss of contact from times 0.7 to 0.9 ms. The panel center then reaches its maximum displacement of 9.7 mm and, in rebounding, pushes the ice mass backwards with a nontrivial amount of force, as indicated by the second force pulse. Finally, the ice mass is completely ejected away from the panel at 1.5 ms, before the second displacement peak is reached.

Figure 13 shows the predicted panel strain histories at locations SG1 (backside, center) and SG2 (backside, 25.4 mm from center) for simulation of test 137 (42.7-mm SHI at 73.2 m/s). As seen in Fig. 13, the FE model closely predicts the center strain gauge SG1 history. The peak strain, time to peak, and general overall trend matches with the experimentally measured strain. At location SG2, the DYNA3D prediction does not match the experimental strain as closely when results are taken at 25.2 mm (location of element center closest to 25.4 mm) from the panel center. However, when model results are taken at a distance of 16.3 mm from the panel center, the test data are predicted quite well.

A simple explanation for this mismatch is that the ice sphere impacted the panel 9.1 mm (25.4 − 16.3 mm) from the center. This reason is ruled out because the data of strain gauge SG1 are predicted so closely when FE model results are taken at the panel center, and not at 9.1 mm from center. Another explanation is that the ice sphere material model behavior is overly stiff. Note that the predicted panel center deflection response (see Fig. 12) occurs at a faster time scale than the data. It is conceivable that the stiffer ice behavior forces

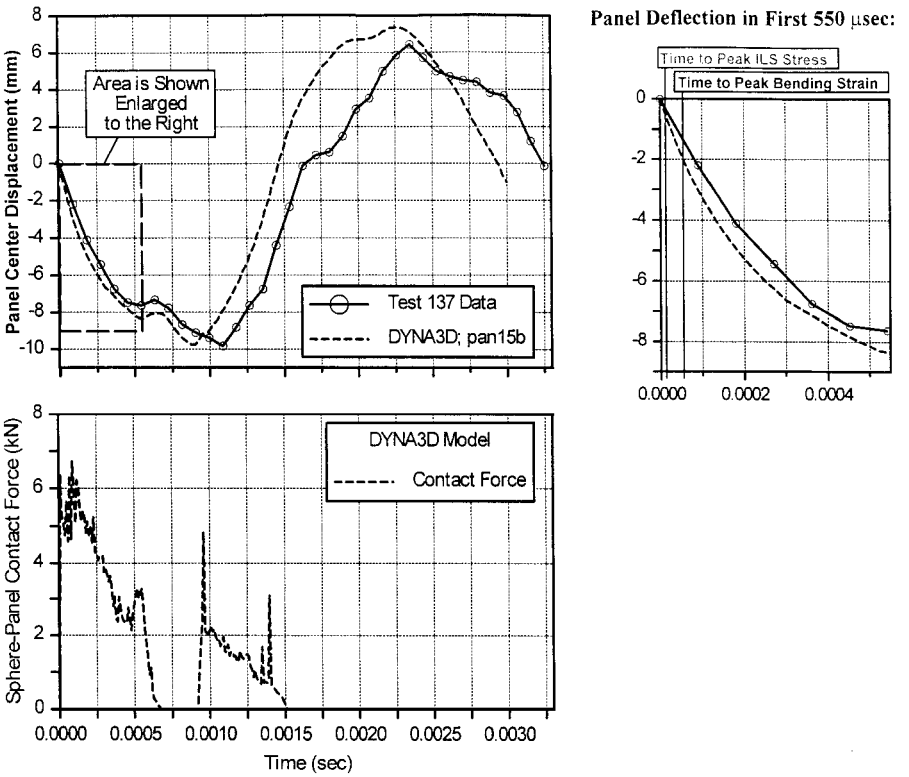

Fig. 12 Panel center deflection and contact force prediction.

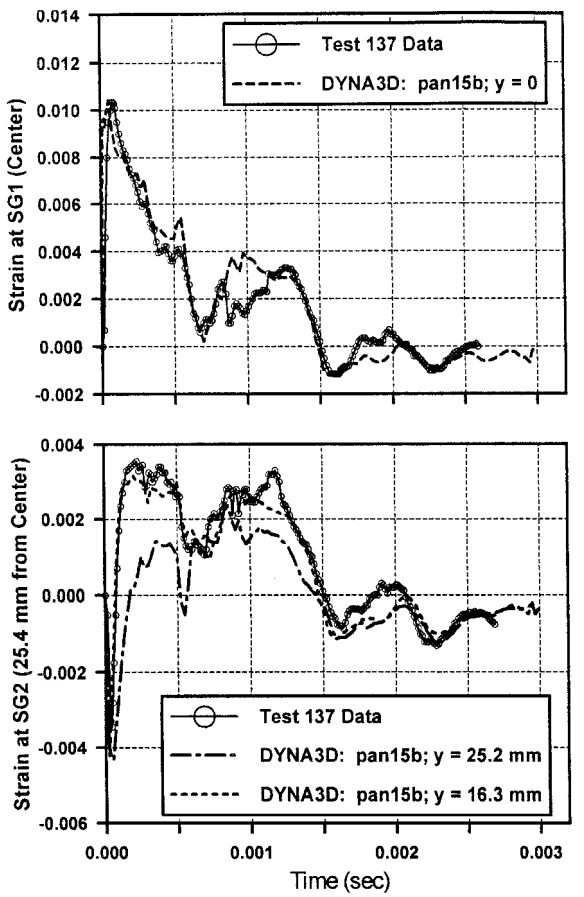

Fig. 13 Predicted strain history and test 137 data; 42.7-mm SHI at 73.2 m/s.

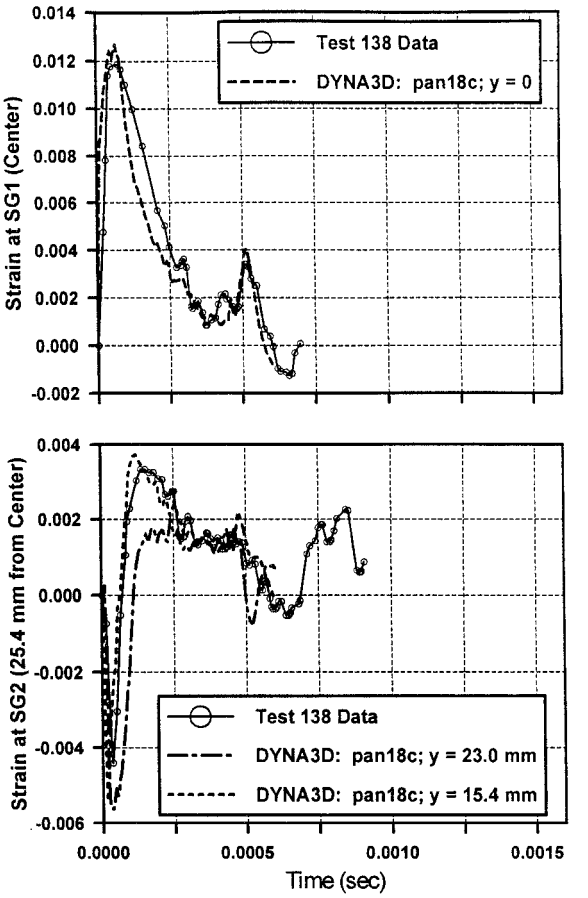

Fig. 14 Predicted strain history and test 138 data; 25.4-mm SHI at 154 m/s.

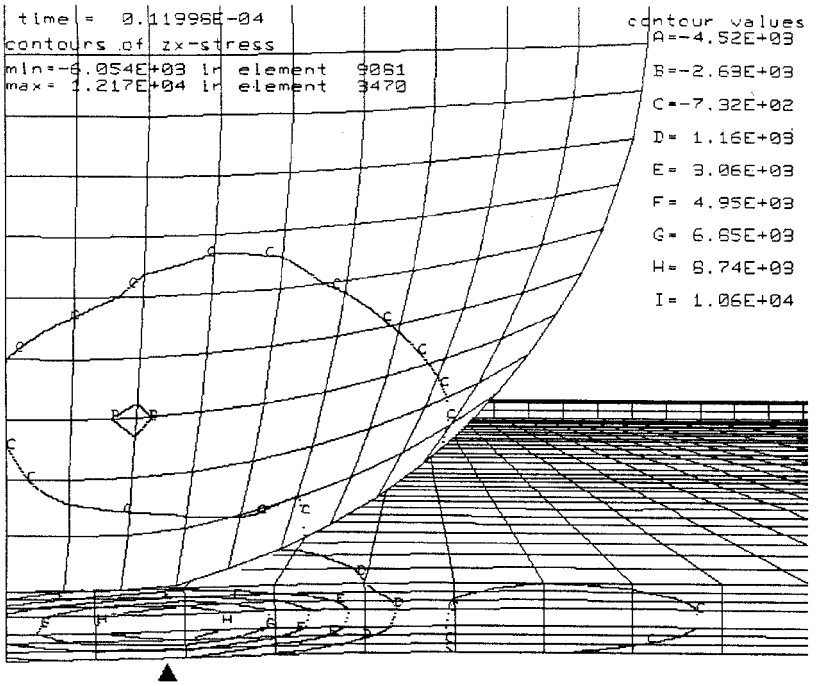

Fig. 15a DYNA3D model pan15b contour plot of τ_{xz} at time $t = 12\,\theta$ s, maximum $\tau_{xz} = 83.9$ MPa (12,170 psi).

a more localized panel deformation response, and, thus, the strain predictions for the gauge SG2 correlate better when model results are taken closer to the impact site. Finally, the aspect ratio of the solid elements used to model the plate is nonideal and is likely a source of error when predicting stress components (or surface strain) near the impact location where high gradients in the in-plane direction exist. Ultimately, the panel's global response can be affected for this reason, which is also a possible explanation for why the predicted panel deformation history diverges from the measured response after a time of 1.5 ms (see Fig. 12).

Figure 14 shows similar predictions of strain gauge data for simulation of test 138 (25.4-mm SHI at 154 m/s). In this case, higher peak strains were predicted and measured for both gauge locations, with first peak values occurring earlier than in test 137.

Close correlation between model predictions and measurable experimental data (i.e., deflection and surface strain at panel center) has been demonstrated. Further information that cannot feasibly be experimentally measured can now be taken from the model with confidence. The sphere-to-panel contact force discussed earlier is one such measure. A metric-to-gauge panel failure, such as ILS stress, can also be obtained from the FE model.

Figure 15a shows a close-up view of the sphere impacting onto the composite panel for model pan15b simulating test 137. Figure 15a displays contours of ILS stress τ_{xz} at a time of 12 μs, which is when peak τ_{xz} is predicted to occur. A dark triangle points out the location of the peak τ_{xz} stress. Contour plots of τ_{xz} at 6 and 18 μs (not shown) allow the observation that the peak τ_{xz} stress moves outward, away from the center of the plate as time progresses. This stress is always a maximum at the boundary of the contact patch that the ice makes as it crushes onto the panel. Additionally, during the timescale in which peak τ_{xz} is developed, the through-the-thickness profile of τ_{xz} of is close to parabolic, with the maximum stress located halfway through the panel thickness.

Figure 15b shows a plot of τ_{xz} through-the-panel thickness at the time of peak τ_{xz} as predicted by the DYNA3D model pan15b. This profile is at a location 5 mm from the plate center, corresponding with the location pointed out in Fig. 15a. A parabolic curve fit, based on matching the peak stress, plotted in Fig. 15b, demonstrates that the parabolic transverse shear stress profile, often assumed in shear deformation beam and plate theory, is justified as a good approximation, even for this complex impact problem. Figure 15c shows the profile of τ_{xz} through the thickness of the panel for the model pan18c. Similar to Fig. 15b of model pan15b, the content of Fig. 15c

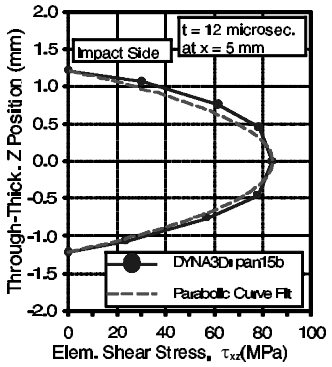

Fig. 15b DYNA3D model pan15b τ_{xz} profile through panel thickness at time of peak stress ($t = 12\,\theta$ s), 42.7-mm ice at 73.2 m/s.

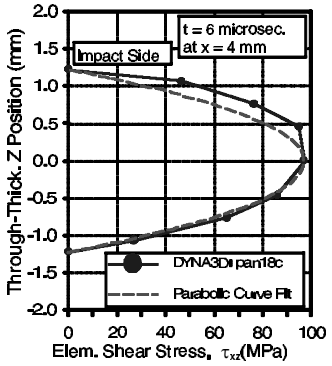

Fig. 15c DYNA3D model pan18c τ_{xz} profile through panel thickness at time of peak stress ($t = 6\,\theta$ s), 25.4-mm ice at 154 m/s.

reaffirms that the ILS stress profile can be well approximated by an assumed parabolic function.

ILS stress is considered here to be the primary driving force for the formation of impact-induced delamination.[5] Figure 16 shows the predicted peak ILS stress component τ_{xz} as a function of time for both DYNA3D models. This is the maximum value of shear stress in any one of the elements used to model the composite panel during the simulation. Thus, the profiles in Fig. 16 are not the τ_{xz} histories of a single element, but of the particular element having the peak τ_{xz} at a given time. Note the order of magnitude difference in timescale between the time at which τ_{xz} peaks, the time to achieve peak surface

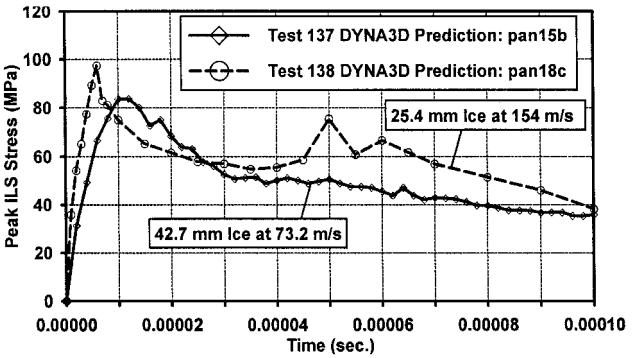

Fig. 16 Peak ILS stress τ_{xz} history for two simulations.

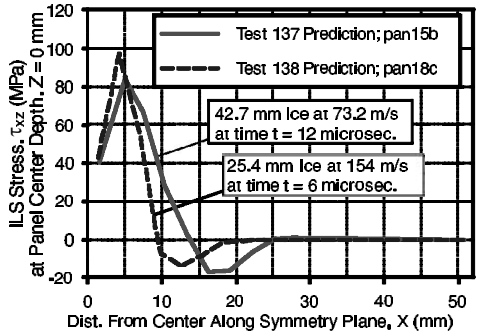

Fig. 17 ILS stress τ_{xz} as a function of distance from impact location.

Table 4 DYNA3D models results summary

DYNA3D model identification	Peak τ_{xz}, MPa	Time to peak, μs	Peak SG1 strain, $\mu\varepsilon$	Time to peak, μs
pan15b[a]	83.9	12	10,430	54
pan18c	97.5	6	12,700	65

[a]See times for model pan15b illustrated in Fig. 12.

strain, and the time to achieve peak panel center deflection (see Figs. 12–14 and 16).

Figure 17 shows the profile of τ_{xz} as a function of position away from the panel center, at the time of peak τ_{xz} stress. The stress is taken from elements at the middepth location along the symmetry plane defined by the x and z axes (see Fig. 5 for axis definitions). In Fig. 17, the results of both DYNA3D models show τ_{xz} to be quite localized near the location of impact during the time in which peak τ_{xz} occurs. Beyond a 25-mm distance from the impact location, τ_{xz} is zero. Note that the panel boundaries are at a 133.4-mm distance away from the impact location, and, thus, at the time of peak τ_{xz} the panel boundaries are not yet aware of the presence of the impacting ice sphere.

Table 4 is a summary of the results for DYNA3D models pan15b and pan18c. Listed are the numerically predicted peak τ_{xz} and peak surface strain at the location SG1 (panel backside center) along with the times to peak τ_{xz} and peak surface strain. Comparison of these times emphasizes that the ILS stress τ_{xz} peaks well before the primarily bending-induced surface strain. In other words, the panel will always experience an interlaminar failure, such as delamination, before fiber failure. This sequence of material failure progression during impacts (i.e., matrix failure before bending induced fiber failure) was also reported by Elber.[12] Finally, Table 4 shows that smaller-diameter, higher-velocity ice projectiles produce higher ILS stress and bending strain in less time. Therefore, an impact by a smaller-diameter ice sphere is more severe than an equivalent energy impact involving a larger-diameter sphere (fired at lower velocity to achieve same kinetic energy due to higher mass).

Failure Threshold Energy Level Prediction

The numerical models have shown that the ILS stress peaks at a time well in advance of the time needed to develop maximum bending strain on the surface of the plate, thus indicating delamination to be the initial failure mode once the FTE level is exceeded. A global energy balance was performed on the system to establish a relationship between the FTE and the experimental parameters. Figure 18 depicts the plate impact problem at a state just before impact and at a state early on during the impact event, specifically, at the time during which peak ILS stress occurs. Just before impact, state 1, the only energy in the system is the kinetic energy T_1 of the ice sphere of mass m that travels at an initial velocity v_0:

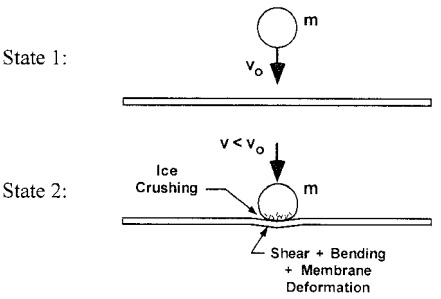

Fig. 18 Energy balance for plate impact problem.

$$E_1 = T_1 = \tfrac{1}{2}mv_0^2 \tag{1}$$

During the impact event, state 2, the ice (still having mass m) is at a reduced velocity v that is expressed as a proportion of the initial velocity, that is, $v = \alpha v_0$ $(0 < \alpha < 1)$. At state 2, the total energy in the system is a combination of the sphere's remaining kinetic energy plus the energy stored by elastic deformations in the plate and ice sphere:

$$E_2 = T_2 + V_2 = \tfrac{1}{2}mv^2 + V_{\text{shear}} + V_{\text{other}} \tag{2}$$

V_{shear} is the energy due to shear deformation of the plate. V_{other} accounts for the other sources of elastic energy storage such as the bending and membrane deformation in the plate and the elastic energy stored in the ice sphere.

An energy balance can now be written using Eqs. (1) and (2):

$$E_2 - E_1 = W_{\text{nc}} \tag{3}$$

where W_{nc} is the nonconservative work that occurs in passing from states 1 to 2. This term is primarily the work performed due to the local crushing of the ice sphere near the location of sphere-to-panel contact. It also accounts for energy loss due to friction and sound.

The strain energy due to shear deformation can be expressed using a volume integral over the portion of the plate in which shear deformation occurs. From the DYNA3D models, it has been shown that during the time frame in which peak ILS stress develops, the panel deformations are small (see Fig. 12) and quite localized near the point of impact (see Fig. 17). Calculation of the shear deformation energy is difficult due to the complex distribution τ_{xz} has through the panel thickness and the in-plane coordinates, the latter distribution being shown schematically in Fig. 19 at the panel center-depth location. A simplifying approximation can be made by assuming an average value of shear stress τ_{av} throughout the portion of panel volume that is affected by the sphere impact. This allows for a simple relationship for the shear strain energy to be composed:

$$V_{\text{shear}} = \frac{1}{2}\int_{\text{Vol}} \frac{\tau_{xz}^2}{G_{xz}}\,\text{dVol} = \frac{\tau_{\text{av}}^2}{2G_{xz}}\pi H\left(\frac{\beta D}{2}\right)^2 \tag{4}$$

where τ_{av} is the average stress, G_{xz} is the interlaminar shear modulus of the composite panel, βD is the diameter of volume over which the average shear stress acts (β is a proportionality constant, and D is the sphere diameter), and H is the thickness of the panel; the volume is assumed to be a simple plug.

Substituting Eqs. (1), (2), and (4) into Eq. (3), making the substitution of $v = \alpha v_0$ stated earlier, and recognizing that the initial kinetic energy, $KE_0 = \frac{1}{2}mv_0^2$, we can rewrite the energy balance as

$$KE_0 = \frac{1}{1-\alpha^2}\left[\frac{\tau_{\text{av}}^2}{8G_{xy}}\pi\beta^2 D^2 H + V_{\text{other}} - W_{\text{nc}}\right] \tag{5}$$

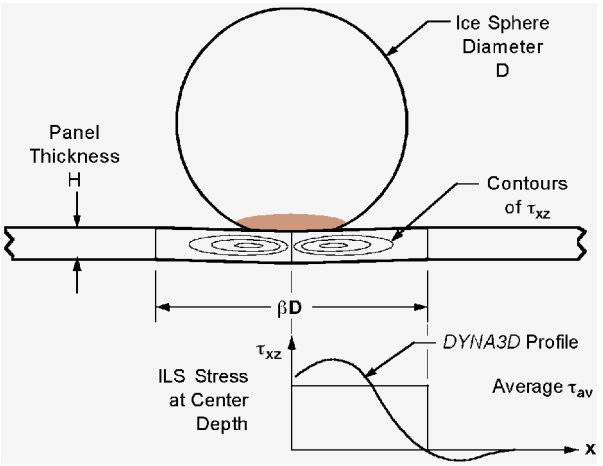

Fig. 19 Panel shear deformation and ILS stress profile.

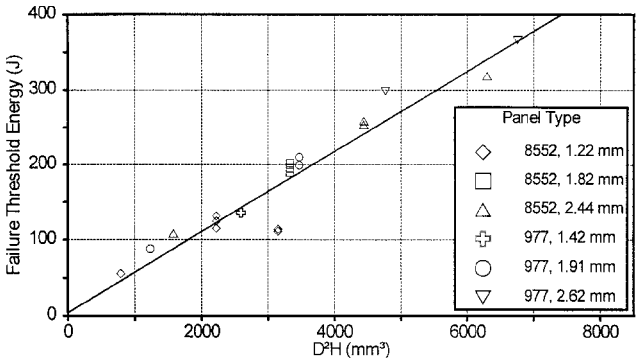

Fig. 20 Summary of panel failure threshold energy for all tests.

Within the timescale to which the ILS stress peaks, it shall be assumed that the terms V_{other} and W_{nc} are small compared to the magnitudes of the shear deformation energy and kinetic energy terms. These terms can be considered as constants due to their minor contributions, despite there being some functional dependence of these variables on the geometric parameters H and D. Observing Eq. (5), α and β are both proportionality constants, indicators of the amount of velocity reduction and sphere deformation, respectively. The only controllable experimental parameters remaining that would relate the kinetic energy to the average shear stress are panel thickness H and sphere diameter D. Finally, consider the case in which the projectile has just enough initial kinetic energy to initiate a delamination failure. The average shear stress would be at some critical value, τ_{av}^{crit}, and the kinetic energy KE_0 would be the FTE discussed earlier. Making these substitutions into Eq. (5),

$$\text{FTE} = \frac{1}{1-\alpha^2}\left[\frac{\left(\tau_{av}^{crit}\right)^2}{8G_{xy}}\pi\beta^2 D^2 H + V_{other} - W_{nc}\right] = C_1 + C_2 D^2 H \tag{6}$$

The parameters C_1 and C_2 can be empirically determined. Equation (6) establishes the functional form in which FTE is related to the geometric parameters H and D. The data in Table 1 are plotted in Fig. 20 in accordance to Eq. (6), that is, FTE vs D^2H. All of the experimental data collapses under this single relationship for the entire range of test conditions. The linear fit to the data, following the form of Eq. (6), indicates that C_1 and C_2 are independent of D and H and are empirically determined constants over the range of ice impact velocities tested. Having established this functional relationship, the FTE can be predicted for any combination of ice diameter and panel thickness, within the requirement that the impact occurs at high velocity and that the ice sphere fails in a similar manner as tested.

Discussion

Panel impact experiments have shown that a sequence of failure modes can exist over a range of test velocities and that the severity of damage does not always increase with increasing severity of impact, that is, higher velocity for a given sphere diameter.

In support of the panel impact simulations, an ice projectile material model was first developed by modeling the case of ice impacting the instrumented FMT system. From these initial FMT models, the following conclusions can be drawn: 1) The kinematic behavior of the FE models matches the experimentally observed ice failure behavior. 2) The linear trend of peak force vs projectile kinetic energy, as predicted by the DYNA3D simulations, matches the experimental data for SHI of monolithic construction (slopes within 1% of each other). 3) Over the studied range of velocity, 30–200 m/s, impact ice material can successfully be modeled using the DYNA3D material type 13 elastic–plastic with failure model without accounting for complex pressure-volumetric behavior and failure strength sensitivity to strain rate and pressure. This model, once developed, can be readily applied to simulate ice impacts onto any target.

Predictions of the panel center deflection history matched to within 0.7% of experimental measurement for the first peak of the oscillatory response, but were off by 14% for the second peak. This discrepancy is of little consequence when predicting damage because significant levels of surface strain were measured to exist only during the period of 1.5 ms after first contact. Beyond this time, the sphere and panel have lost contact and the panel is freely vibrating. Thus, it is hypothesized that any damage formation in the panel would occur only during the time in which sphere-to-panel contact exists. Furthermore, the models have shown that the time to reach peak ILS stress (potentially causes delamination) occurs several times earlier than the time to reach peak bending strain (causes fiber failure), which itself occurs at a time scale two orders of magnitude lower than the time to reach the first peak in panel deformation. Thus, the models reinforce the experimental observations that the delamination failure is the initial failure mode and that it occurs before bending-induced fiber failure.

The peak force during contact of the ice with the panel occurs almost immediately, as well as peak ILS stress and surface strain. Additionally, the contact patch is initially small, indicating that very high contact pressure, and ILS stress develops locally at the impact location, before significant deformations occur throughout the plate. Thus, the failures observed experimentally had developed, or at least initiated, locally to the region of impact, and their initial formations were not strongly influenced by the panel boundary conditions. Observe also that the time of peak contact force does not coincide with the time of peak panel displacement. The panel center reaches maximum displacement at a time when the contact force is momentarily zero. This observation emphasizes that these impacts are high-velocity and must be considered as dynamic problems. If dynamic phenomena were not an important factor in the panel response, then peak contact force and maximum panel center displacement would be coincident in time, as is often the case in low-velocity, that is, drop tower, impacts. Therefore, simple quasi-static-based global analyses, common and valid when dealing with low-velocity impacts, cannot be applied to this class of problems.

An apparent contradiction exists between this last statement and those made regarding the static punch-type parabolic ILS stress profile developed as the sphere impinges onto the panel. This conflict is addressed by considering the importance of timescales governing each mode of panel response; consider global deflection vs local stress buildup. A simple wave speed calculation shows the transit time for a shear wave to pass through the panel thickness to be on the order of 1.3 μs. The time to develop peak ILS stress is 12 μs, an order of magnitude larger timescale, giving the through-thickness ILS stress time to develop into a quasi-static-like profile. Therefore, treating the ILS stress distribution local to the sphere-to-panel contact boundary in a quasi-static manner is justified, as well as confirmed by the numerical results.

The numerical modeling results assisted in making assumptions and simplifications in the formulation of an energy balance relationship that predicts the FTE as a function of geometric experimental parameters. The experimentally measured FTE data, when plotted

in accordance to the functional form of this relationship, indicated a single linear relationship between the FTE and the grouping of geometric parameters D^2H, with only two empirically determined constants to be found. Once established, the form of this relationship can then be applied to facilitate prediction of the ice impact damage resistance for any material system using a relatively low number of tests. Furthermore, due to the timescale within which the ILS stress peaks, panel deflections remain quite localized, and the relationship is, therefore, independent of panel boundary conditions and can be directly applied to predicting damage initiation in composite structures of similar gauge thickness when impacted by ice at high velocities. Finally, it is proposed that this damage resistance prediction method presented can be applicable to other forms of impact as well as ice, such as impacts by elastomeric or even metallic projectiles. Further verification is needed, however, to validate this hypothesis.

Conclusions

Experiments of ice impacting the FMT show that a linear relationship exists between a high-velocity ice projectile's kinetic energy and the measured peak force. It is expected that this type of relationship would exist for high-velocity ice projectile impacts onto any target, i.e., real structures, under the condition that similar ice failure modes result in all of the tests (i.e., localized crushing). For impacts of ice onto composite panel targets, experiments have shown that a progression of failure modes exists, starting with delamination as the initial failure mode after the impact damage resistance threshold is surpassed.

The numerical simulations have shown that ice impact models can successfully represent high-velocity ice while impacting a structure. The insights afforded by validated simulation allow the conclusions that significant levels of ILS occur well before bending-induced surface strain, thus challenging the interlaminar strength of a composite panel target before challenging the fiber in-plane breaking strength. This supports the observation of delamination as the initial mode of failure. Additionally, the experiments and modeling show that a smaller-diameter projectile is more severe than one of larger diameter when impacting an identical panel target at the same level of projectile kinetic energy.

A combination of the insights gained from the numerical simulations and the experimental measurements allowed the formulation of an analytical prediction of the projectile kinetic energy at which failure initiates, i.e., the FTE. Because these high-velocity impacts result in a localized target response during the time frame in which failure of the panel can occur, the boundary conditions of a panel impact test do not influence damage initiation, and thus this predictive formula can be applied to establish the ice impact damage resistance of any actual composite structure of similar panel thickness.

Acknowledgments

This work was supported through the Defense Advanced Research Projects Agency–funded and Pratt and Whitney–led Affordable Composites for Propulsion Program. All DYNA3D computations were run on the National Partnership for Advanced Computational Infrastructure San Diego Supercomputer Center Cray T90.

References

[1]Jackson, W. C., and Poe, C. C., Jr., "The Use of Impact Force as a Scale Parameter for the Impact Response of Composite Laminates," NASA TM-104189, Jan. 1992; also Army Aviation Systems Command, TR 92-B-001, Jan. 1992.

[2]Greszczuk, L. B., "Damage in Composite Materials Due to Low Velocity Impact," *Impact Dynamics*, edited by J. A. Zukas, T. Nicholas, H. F. Swift, L. B. Greszczuk, and D. R. Curran, Wiley, New York, 1982, pp. 55–94.

[3]Shivakumar, K. N., Elber, W., and Illg, W., "Prediction of Impact Force and Duration Due to Low-Velocity Impact on Circular Composite Laminates," *Journal of Applied Mechanics*, Vol. 52, No. 3, 1985, pp. 674–680.

[4]Sjöblom, P., "Simple Design Approach Against Low-Velocity Impact Damage," *Proceedings of the 32nd International SAMPE Symposium*, Society for the Advancement of Material and Process Engineering, Covina, CA, 1987, pp. 529–593.

[5]Joshi, S. P., and Sun, C. T., "Impact Induced Fracture in a Quasi-Isotropic Laminate," *Journal of Composites Technology and Research*, Vol. 9, No. 2, 1987, pp. 40–46.

[6]Joshi, S. P., and Sun, C. T., "Impact Induced Fracture in a Laminated Composite," *Journal of Composite Materials*, Vol. 19, No. 1, 1985, pp. 51–66.

[7]Guynn, E. G., and O'Brien, T. K., "The Influence of Lay-Up and Thickness on Composite Impact Damage and Compression Strength," *Proceedings of the AIAA/ASME/ASCE/AHS 26th Structures, Structural Dynamics, and Materials Conference*, AIAA, New York, 1985, pp. 187–196.

[8]Singh, S., Masiulaniec, K. C., DeWitt, K. J., and Britton, R. K., "Measurements of the Impact Forces of Shed Ice Striking a Surface," AIAA Paper 94-0713, Jan. 1994.

[9]Jones, S. J., "High Strain-Rate Compression Tests on Ice," *Journal of Physical Chemistry B*, Vol. 101, No. 32, 1997, pp. 6099–6101.

[10]Schulson, E. M., "The Brittle Failure of Ice Under Compression," *Journal of Physical Chemistry B*, Vol. 101, No. 32, 1997, pp. 6254–6258.

[11]Kim, H., "The Damage Resistance of Composite Structures to High Velocity Ice Impacts and Their Tolerance to Impact Damage," Ph.D. Dissertation, Dept. of Mechanical and Environmental Engineering, Univ. of California, Santa Barbara, CA, Dec. 1998.

[12]Elber, W., "The Effect of Matrix and Fiber Properties on Impact Resistance," *Tough Composite Materials*, Noyes, Park Ridge, NJ, 1985, pp. 89–110.

[13]Ghaffari, S., Tan, T.-M., and Awerbuch, J., "An Experimental and Analytical Investigation on the Oblique Impact of Graphite/Epoxy Laminates," *Proceedings of the 22nd International SAMPE Technical Conference*, Society for the Advancement of Material and Process Engineering, Covina, CA, 1990, pp. 494–508.

[14]Whirley, R. G., and Engelmann, B. E., "DYNA3D: A Nonlinear, Explicit, Three-Dimensional Finite Element Code for Solid and Structural Mechanics—User Manual," Lawrence Livermore National Lab., UCRL-MA-107254 Rev. 1, Livermore CA, Nov. 1993.

[15]Batto, R. A., and Schulson, E. M., "On the Ductile-to-Brittle Transition in Ice Under Compression," *Acta Metallurgica et Materialia*, Vol. 41, No. 7, 1993, pp. 2219–2225.

[16]Schulson, E. M., "The Brittle Compressive Fracture of Ice," *Acta Metallurgica et Materialia*, Vol. 38, No. 10, 1990, pp. 1963–1976.

[17]Mellor, M., "Mechanical Properties of Polycrystalline Ice," *Physics and Mechanics of Ice*, edited by P. Tryde, Springer-Verlag, New York, 1980, pp. 217–245.

[18]Schroeder, R. C., and McMaster, W. H., "Shock-Compression Freezing and Melting of Water and Ice," *Journal of Applied Physics*, Vol. 44, No. 6, 1973, pp. 2591–2594.

[19]Mellor, M., and Cole, D. M., "Deformation and Failure of Ice Under Constant Stress or Constant Strain-Rate," *Cold Regions Science and Technology*, Vol. 5, No. 3, 1982, pp. 201–219.

[20]Nadreau, J. P., Mawwar, A. M., and Wang, Y. S., "Triaxial Testing of Freshwater Ice at Low Confining Pressures," *Proceedings of the Seventh International Conference on Offshore Mechanics and Arctic Engineering*, American Society of Mechanical Engineers, New York, 1988, pp. 117–124.

A. M. Waas
Associate Editor